Supporting Information

Construction of superhydrophilic FeP-Ni_2P-CoP/NF enriched interfacial heterostructures for promoting efficient and stable overall water splitting under large currents

Yaxuan Jin[a], Weiyan Ma[a], Dong Sun[a], Wan Wan[a], Lirong Jia[a], Yuling Tu[a], Dejun Gong[a], Wanyong, Zhou[b], Hui Chai[a,*]

[a]State Key Laboratory of Chemistry and Utilization of Carbon Based Energy Resources, Key Laboratory of Energy Materials Chemistry, Ministry of Education; College of Chemistry, Xinjiang University, Urumqi, 830017, Xinjiang, PR China

[b]College of Chemical Engineering, Xinjiang University, Urumqi, Xinjiang, PR China

[*]Corresponding author: Tel: +86 9918583083; Fax: +86 9918588883; E-mail: huichmails@163.com

Experimental section

Chemicals

Cobalt(II) nitrate hexahydrate ($Co(NO_3)_2·6\ H_2O$), nickel (II) nitrate hexahydrate ($Ni(NO_3)_2·6\ H_2O$),Iron (III) nitrate nonahydrate ($Fe(NO_3)_3·9\ H_2O$) , ammonium fluoride (NH_4F), urea ($CO(NH_2)_2$), potassium hydroxide (KOH)and Ethanol (C_2H_5OH)were purchased from Sinopharm Chemical Reagent Co., Ltd (Shanghai, China). Pt/C (20 wt.%) and ruthenium (IV) oxide (RuO_2) were purchased from Alfa Aesar. Nafion (5 wt.%) was purchased from Sigma-Aldrich Sodium. Hypophosphite (NaH_2PO_2) was purchased from Aladdin. All chemical regents were used as received without further purification. Nickel foam (NF) was purchased from Kunshan Shengshijing New Materials Co., Ltd (Kunshan, China).

Synthesis of Fe-$Ni(OH)_2$-$Co(OH)_2$/NF catalyst

Nickel foam (4.0×4.0 cm^2) was sonicated in 1.0 M HCl aqueous solution for 15 min to remove surface impurities, washed to neutrality and then sonicated with deionized water and anhydrous ethanol alternately for 10 min. The cleaned nickel foam was dried in vacuum at 60℃

for 8 h for reserve.

First, 0.8731 g of ($Co(NO_3)_2$·6 H_2O), 0.2908 g of $Ni(NO_3)_2$·6 H_2O, 0.2828 g of $Fe(NO_3)_3$-9 H_2O, 0.0741 g of NH_4F, and 0.2402 g of urea were added to 25 mL of deionized water. A piece of pretreated NF (1.5 cm × 3 cm) was added with magnetic stirring for 30 min and transferred to a Teflon-lined autoclave. The autoclave was heated at 150°C for 6 hours. After cooling naturally to room temperature, the sample was washed three times with deionized water and ethanol, and dried under vacuum at 60°C for 8 h. The synthesized sample was noted as Fe-$Ni(OH)_2$-$Co(OH)_2$/NF. For comparison, $Ni(OH)_2$-$Co(OH)_2$/NF was prepared in the same way as Fe-$Ni(OH)_2$-$Co(OH)_2$/NF except that no iron source was added. $Ni(OH)_2$/NF , $Co(OH)_2$/NF and $Fe(OH)_3$/NF were prepared in a similar manner.

Synthesis of FeP-Ni_2P-CoP/NF catalyst

The Fe-$Ni(OH)_2$-$Co(OH)_2$/NF precursor and 2.0 g of NaH_2PO_2 were placed in a tube furnace, with NaH_2PO_2 upstream and the precursor downstream, and then the temperature was increased to 350°C at 2°C min^{-1}, and the temperature was held at 350°C for 2 h to obtain FeP-Ni_2P-CoP/NF.Ni_2P-CoP/NF was prepared in the same way as FeP-Ni_2P-CoP/NF. Ni2P/NF, CoP/NF and FeP/NF were prepared in a similar manner.

Synthesis of Pt-C/NF and RuO_2/NF catalysts

2.5 mg of Pt, add 370 μL of isopropanol, 30 μL of Nafion, 100 μL of deionized water, sonicate for 1 h to obtain a uniformly dispersed ink, drop the prepared ink uniformly onto a clean 1.0 × 1.0 cm^{-2} nickel foam, and dry it at room temperature to obtain Pt-C/NF. RuO_2/NF is prepared in the same way as Pt-C/NF, with the addition of 1 mg of carbon black. The loading of RuO_2/NF and Pt-C/NF was 1 mg cm^{-2}.

Materials characterizations

X-ray diffraction (XRD) measurements were carried out on a Bruker D8 Advance X-ray diffractometer with a Cu Kα source (λ = 1.5406 Å). The morphology and components of the samples were obtained through a field emission scanning electron microscope (SEM, Hitachi S-4800) equipped with an energy dispersive spectrometer (EDS) and transmission electron

microscopy (TEM) with a JEOL JEM-2800. Raman spectra were measured by a Bruker Senterra R200-L spectrometer (532 nm). The electronic states of the samples were investigated by the X-ray photoelectron spectroscopy (XPS, Thermo Fisher Scientific K-Alpha with Al Kα radiation). All binding energies were calibrated by the C 1s peak at 284.8 eV. The contents of Fe, Co, and Ni in the electrolyte after OER were determined by an inductively coupled plasma-optical emission spectrometer (ICP-OES, Agilent 5110). Water contact angle measurements were performed using a Dataphysics OAC 25 instrument. In this context, 3 μL droplets of DI water was adapted as working medium to drop onto sample glass slide to perform contact angle analysis.(or 3 μL n-hexane droplets as working medium.)

Electrochemical measurements

Electrochemical measurements were performed on a CHI 760E electrochemical workstation with a standard three-electrode system. Graphite rod and Hg/HgO electrode were employed as a counter electrode and a reference electrode, respectively. The electrochemical performances were evaluated in 1.0 M KOH solution. All the potentials were calibrated to the reversible hydrogen electrode (RHE) through the following equation:

$$E_{RHE} = E_{Hg/HgO} + 0.098\ V + 0.059pH$$

Linear sweep voltammetry (LSV) were performed at a scan rate of 5 mV s^{-1} by 100%-iR compensation. Electrochemical impedance spectroscopy (EIS) measurements were recorded over a frequency ranging from 100 kHz to 0.1Hz with an potential amplitude of 5 mV at a constant overpotential of 338 mV. The durability test was carried out by taking continuous potential cycling at a scan rate of 100 mV s^{-1} for 5000 cycles. The electrochemical double-layer capacitance (Cdl) was determined from cyclic voltammograms measured in a non-Faradaic region with the scan rates of 20, 40, 60, 80, and 100 mV s^{-1}. The ECSA of the prepared electrocatalysts were evaluated by measuring the Cdl via CV measurements at different scan rates in the potential range without the redox process. The ECSA was derived from the equation: ECSA = Cdl / Cs, where Cs is the specific capacitance. In this work, 0.04 mF cm^{-2} was adopted as the value of Cs. The density of the ECSA-normalized LSV curves was calculated by the equation: ECSA-normalized current

density = current density × Cs / Cdl. The Faradaic efficiencies of the OER and HER on the FeP-Ni_2P-CoP/NF was obtained by the ratio of the amount of O_2 (or H_2) experimentally collected by a drainage method to the amount of corresponding gas theoretically calculated. The overall water splitting tests were performed in a twoelectrode system with the FeP-Ni_2P-CoP/NF as both cathode and anode. For the benchmark noble metal-based catalysts, RuO_2||Pt/C utilized the same mass loading as FeP-Ni_2P-CoP/NF||FeP-Ni_2P-CoP/NF.

Faradaic efficiency calculation

The working electrode was prepared by tailoring the FeP-Ni_2P-CoP/NF electrode with a surface area of 1 cm^2. A constant electrical current at 0.1 A was applied on the electrode and the volume of the evolved gas was recorded synchronously. Thus, the faradaic yield was calculated from the ratio of $V_{\text{experimental}}$ (the recorded gas volume) to $V_{theoretical}$ (the theoretical gas volume) during the charge transport process.

$$Faradaic\ yield = \frac{V_{experimental}}{V_{theoretical}} = \frac{m}{\frac{I}{n} \times \frac{t}{F}} = \frac{m \times F}{I \times t}$$

where m = PΔV/RT (P = P_o-ρgh = 1.01×10^5 Pa-$10^3\times10\times0.1$ Pa=10^5 Pa, ρ is the density of water, h is the height of liquid in graduated cylinder: about 0.1 m, P_o is the atmosphere pressure); ΔV is the change value of gas in graduated cylinder; R is a constant value of 8.314; T is the value of 298 K; F is Faraday constant (96485.3 C mol^{-1}), n =2/4 means 2/4-mole electrons per mole H_2/O_2.

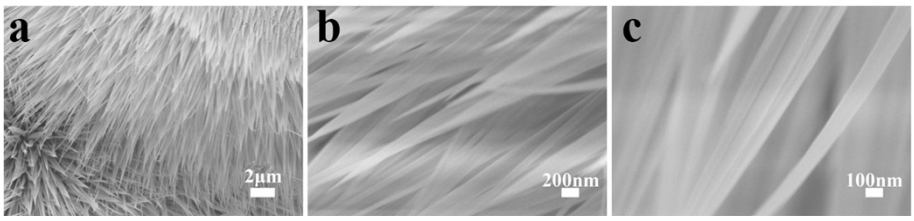

Fig. S1. SEM images of Fe-$Ni(OH)_2$-$Co(OH)_2$ /NF with different magnifications.

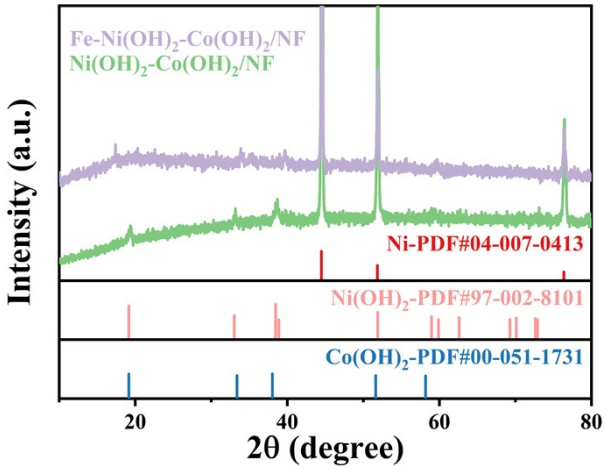

Fig. S2. XRD patterns of Fe-$Ni(OH)_2$-$Co(OH)_2$/NF.

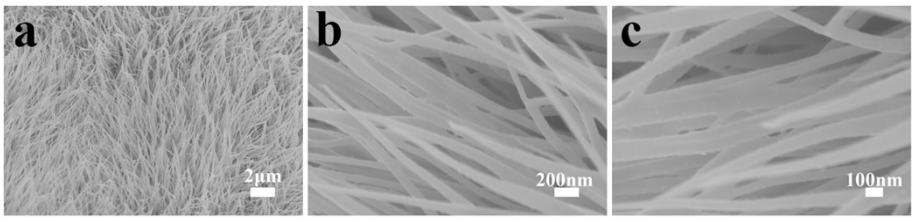

Fig. S3. SEM images of Ni_2P-CoP/NF with different magnifications.

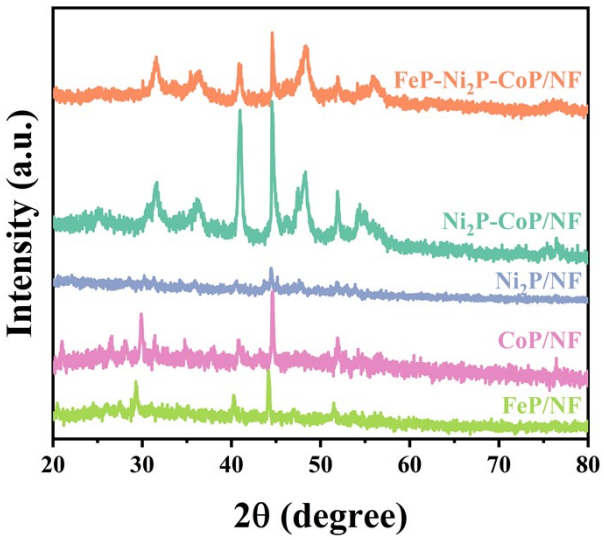

Fig. S4. XRD patterns of FeP-Ni_2P-CoP/NF, Ni_2P-CoP/NF, Ni_2P/NF, CoP/NF and FeP /NF.

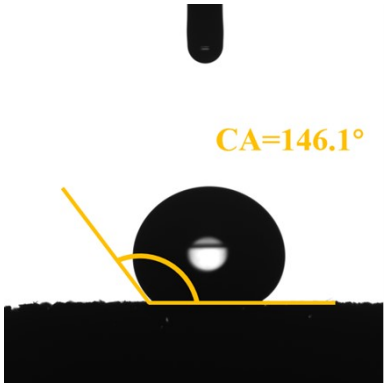

Fig. S5. Lipophilic contact angle of FeP-Ni_2P-CoP/NF.

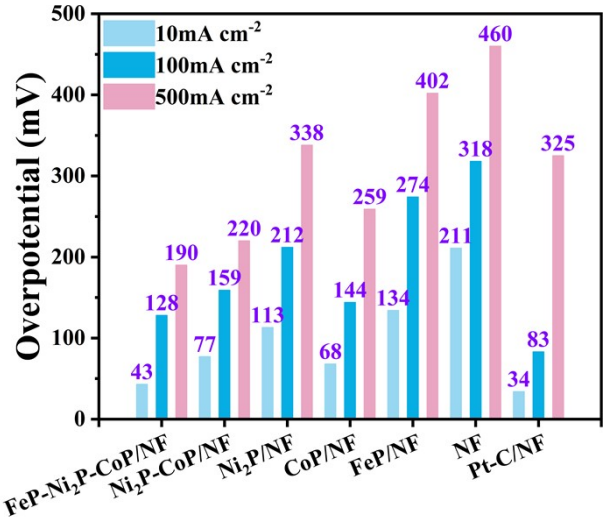

Fig. S6. HER Overpotential at 10, 100 and 500 mA cm^{-2}.

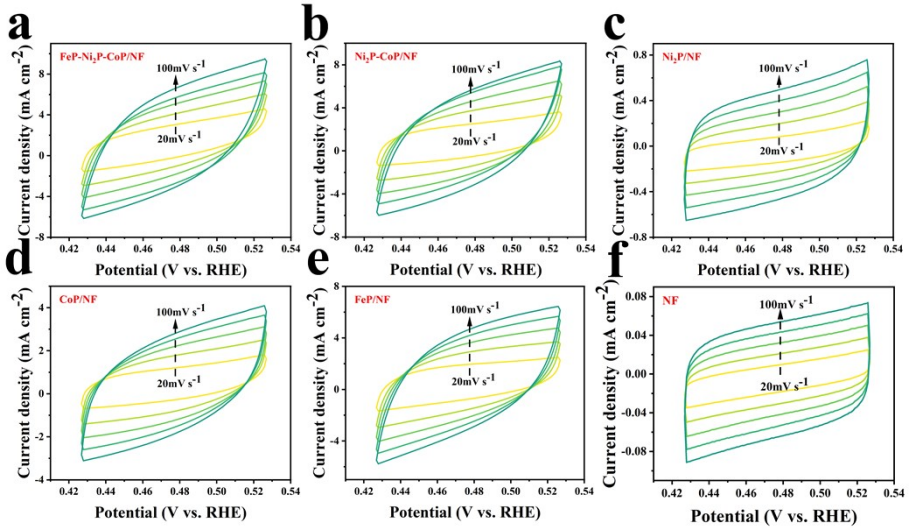

Fig. S7. Cyclic voltammograms (CV) for (a) FeP-Ni_2P-CoP/NF, (b) Ni_2P-CoP/NF, (c) Ni_2P/NF, (d) CoP/NF,(e) FeP/NF, and (f) NF at different scan rate with 20, 40, 60, 80 and 100 mV s^{-1}.

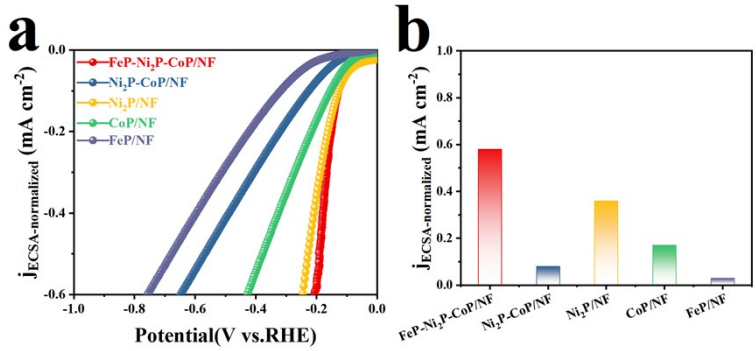

Fig. S8. (a) Specific activities (currents normalized to ECSA) of the FeP-Ni_2P-CoP/NF, Ni_2P-CoP/NF, Ni_2P/NF, CoP/NF, and FeP/NF as a function of applied potential. (b) specific activity at an overpotential of 200 mV.

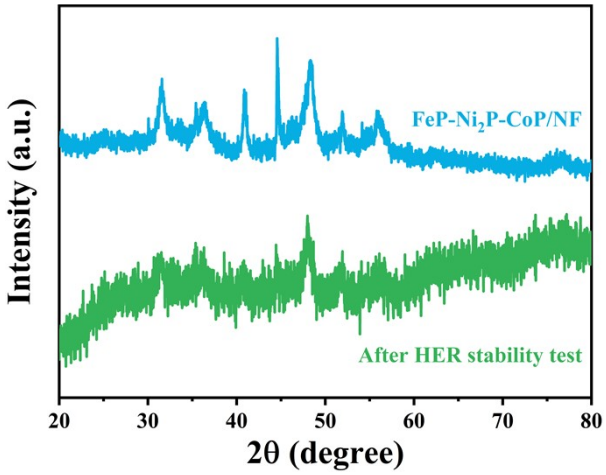

Fig. S9. XRD patterns of FeP-Ni_2P-CoP/NF at initial and after HER stability test.

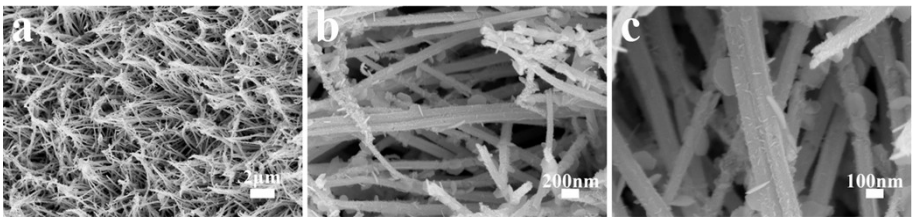

Fig. S10. SEM images of the FeP-Ni_2P-CoP/NF after HER stability test.

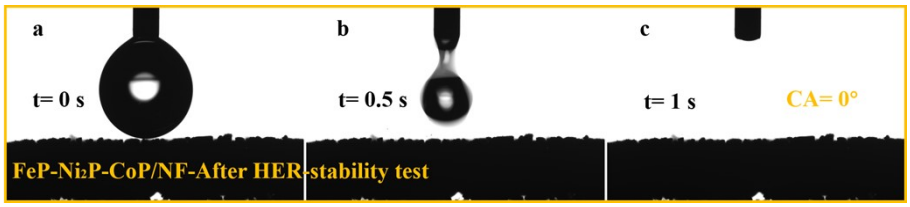

Fig. S11. Wetting characteristics and apparent morphology of FeP-Ni_2P-CoP/NF after HER

stability

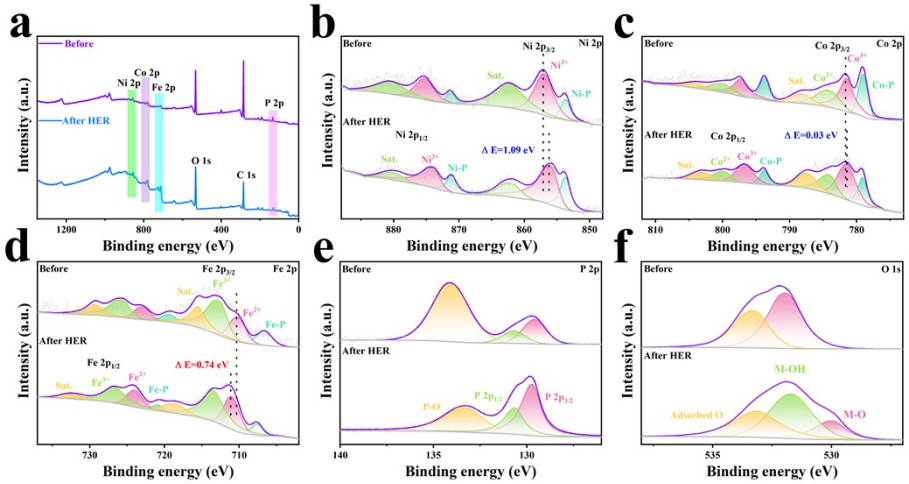

Fig. S12. (a) XPS survey scans of the FeP-Ni_2P-CoP/NF before and after HER stability tests. High-resolution XPS spectra of (b) Ni 2p, (c) Co 2p, (d) Fe 2p, (e) P 2p and (f) O 1s for the FeP-Ni_2P-CoP/NF after HER stability test in 1.0 M KOH.

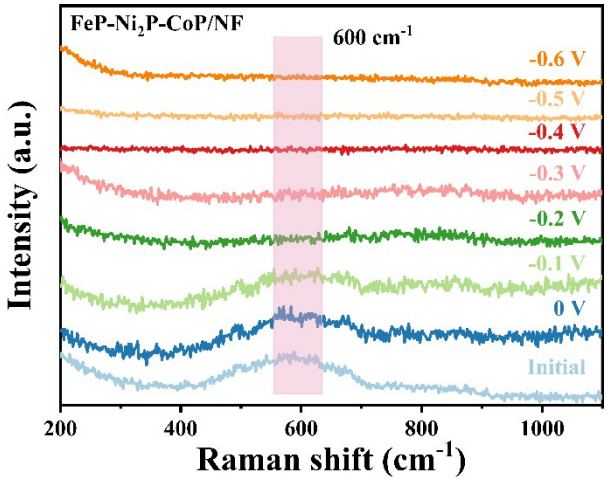

Fig. S13. In situ Raman spectra of FeP-Ni_2P-CoP/NF at various potentials in HER.

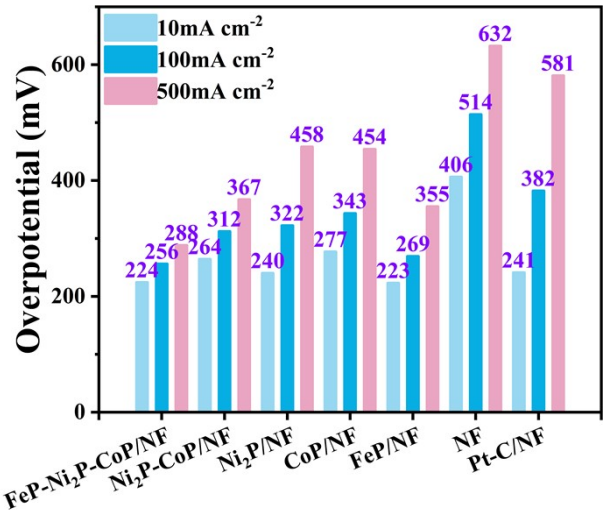

Fig. S14. OER Overpotential at 10, 100 and 500 mA cm^{-2}.

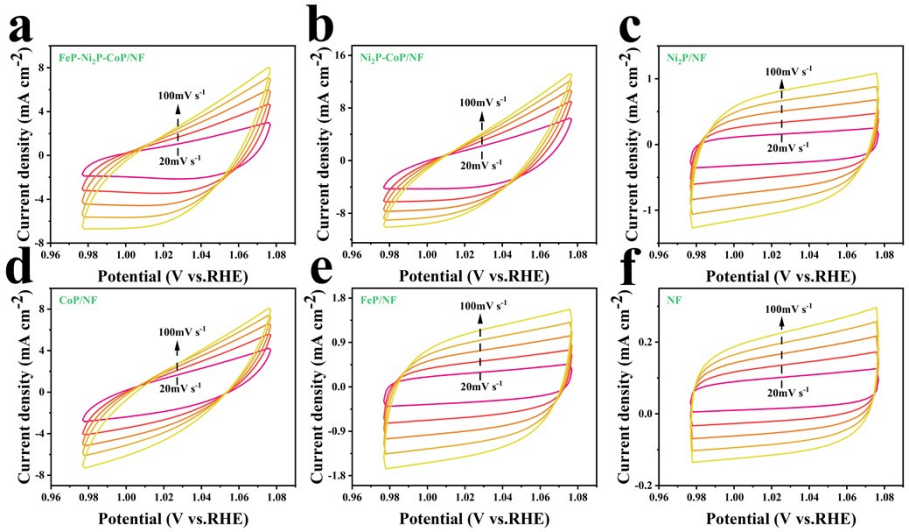

Fig. S15. Cyclic voltammograms (CV) for (a) FeP-Ni_2P-CoP/NF, (b) Ni_2P-CoP/NF, (c) Ni_2P/NF, (d) CoP/NF,(e) FeP/NF, and (f) NF at different scan rate with 20, 40, 60, 80 and 100 mV s^{-1}.

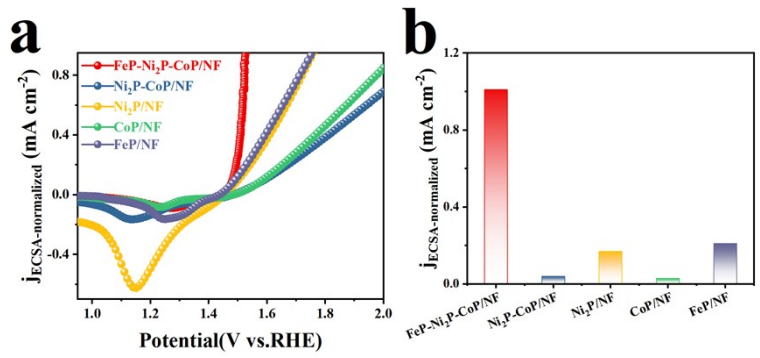

Fig. S16. (a) Specific activities (currents normalized to ECSA) of the FeP-Ni_2P-CoP/NF, Ni_2P-CoP/NF, Ni_2P/NF, CoP/NF, and FeP/NF as a function of applied potential. (b) specific activity at an overpotential of 300 mV.

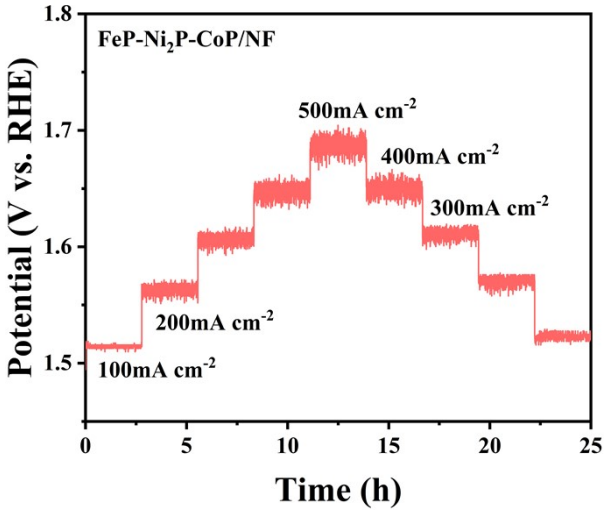

Fig. S17. Multi-step chronopotentiometric curves of FeP-Ni_2P-CoP/NF.

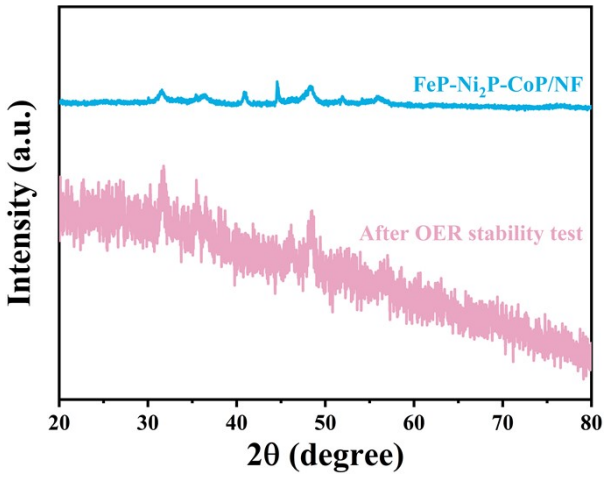

Fig. S18. XRD patterns of FeP-Ni_2P-CoP/NF at initial and after OER stability test.

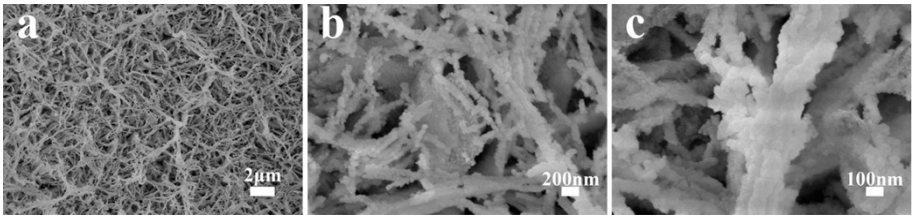

Fig. S19. SEM images of the FeP-Ni_2P-CoP/NF after OER stability test.

Fig. S20. Wetting characteristics and apparent morphology of FeP-Ni_2P-CoP/NF after OER stability

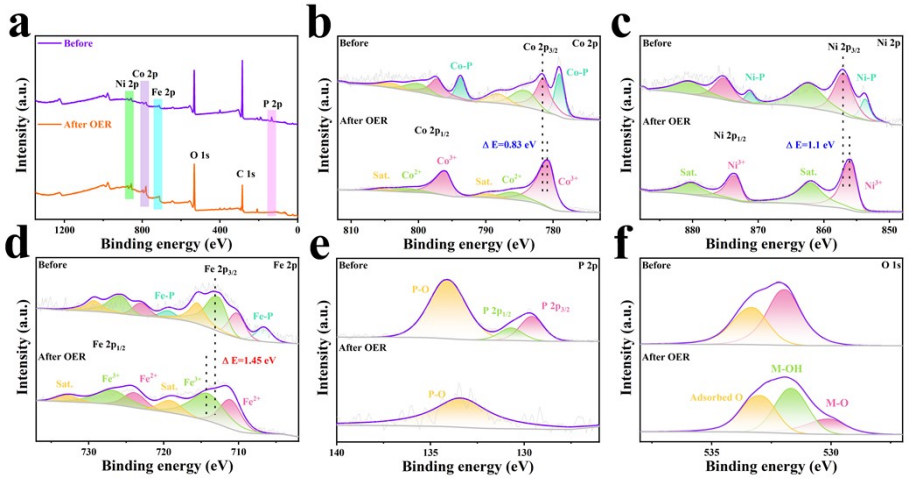

Fig. S21. (a) XPS survey scans of the FeP-Ni_2P-CoP/NF before and after OER stability tests. High-resolution XPS spectra of (b) Co 2p, (c) Ni 2p, (d) Fe 2p, (e) P 2p and (f) O 1s for the FeP-Ni_2P-CoP/NF after OER stability test in 1.0 M KOH.

Video S1. Water contact angles of NF.

Video S2. Water contact angles of FeP-Ni_2P-CoP/NF.

Table S1. Comparisons of HER performances of FeP-Ni_2P-CoP/NF with previously reported nonprecious metal-based and some precious metal-based electrocatalysts in 1.0 M KOH.

Catalysts	Overpotential (mV) at 100 mA cm^{-2}	Tafel slope (mV dec^{-1})	Stability (h) @ J ($mA \cdot cm^{-2}$)	Reference
FeP-Ni_2P-CoP/NF	128	78.47	500@1000	**This work**
Ni/Mo_2C-NCSs	131	66	24@100	[1]
PE-Cr-$CoMoO_4$	131	71.5	24@50	[2]
r-Mn-Ni/CoP	134	43.3	200@100	[3]
NiMoP/NF	135	81.9	100@10	[4]
Fe-CoB_i/CoP/NF	137	75.3	100@50	[5]
CoP/Ni_5P_4/CoP	140	58	21@500	[6]
$CoTe_2$/CoP	148	57	20@100	[7]
FeMoSN@NC	150	67	12@100	[8]
MOF-$Mo_{SA}W_{SA}$	173	82.4	50@100	[9]
Ni-W-P@HFC	180	58.9	70@100	[10]
Mn-W-CoP/NF	184.8	73.4	24@100	[11]
FeCoCrCuO_x@CF	189	27.3	165@500	[12]
CoPϴNPCNTs/CTs	191.1	56	72@20	[13]
CoFe-LDH@NiCoP/NF	196	53.04	100@100	[14]
Mo-Ni_3S_2/NF	199	80.7	100@120	[15]
Ni_2P@C/NF	219	63.8	48@10	[16]
Mo-NiS/Ni_3S_2-0.08S	230	115.7	30@100	[17]
CoNiFe-PS	235	110.58	100@10	[18]
Fe-NiP	252	103.6	24@100	[19]
CoNiCu-LDH@CuO/CF	268	88.4	24@100	[20]

Table S2. Comparisons of OER performances of FeP-Ni_2P-CoP/NF with recently reported nonprecious metal-based catalysts and some precious metal-based electrocatalysts in 1.0 M KOH.

Catalysts	Overpotential (mV) at 100 mA cm^{-2}	Tafel slope (mV dec^{-1})	Stability (h) @ J ($mA \cdot cm^{-2}$)	Reference
FeP-Ni_2P-CoP/NF	256	51.57	500@1000	**This work**
Fe-CoBi/CoP/NF	260	61.9	100@50	5
CoNiFe-PS	263	35.81	100@10	18
$(Fe,Ni)_2P$@Ni_2P	268	56	65@1000	21
Fe-NiP	270	43.6	24@100	19
Mo-NiS_x@NiFe-LDH/NF	271	44.41	72@200	22
P-NiFeMo/NF	274	57.1	72@500	23
CoFe-LDH@NiCoP/NF	275	63.02	100@200	14
H-NMO/CMO/CF-450	281	39.13	300@100	24
CoNiCu-LDH@CuO/CF	286	70.6	24@100	20
CoP@Ni_2P-Fe_2P	287	70	40@100	25
Mo-Ni_3S_2/NF	292	31	100@100	15
Fe/Mo_2C-NCSs	293	86	24@100	1
Ni_2P@C/NF	294	63	48@10	16
$PdFeCo_{3-x}O_4$/NF	300	52	50@500	26
MXene@RuCo NPs	309	61.3		27
MoP-Mo_2C/NPC	330	44.77	90@100	28
Co_2P-Ni_3S_2/NF	332	31.6	48@100	29
Mn-W-CoP/NF	333.2	83.4	100@100	11
CoPϴNPCNTs/CTs	349.1	76.3	72@20	13
$CoTe_2$/CoP	354	89	30@20	7
Ni-W-P@HFC	380	88.3	100@80	10
FeP-350/NF	388	168.7	24@15	30

Table S3. Comparisons of the overall water splitting activity of FeP-Ni_2P-CoP/NF||FeP-Ni_2P-CoP/NF with other electrocatalysts at a current density of 10 mA cm^{-2} in 1.0 M KOH

Catalysts	Potential (V)	Stability (h) @ J ($mA \cdot cm^{-2}$)	Reference
FeP-Ni_2P-CoP/NF	1.5	500@1000	**This work**
MOF-$Mo_{SA}W_{SA}$	1.501	56@500	[9]
CoP@Ni_2P-Fe_2P	1.51	100@500	[25]
NF/O-CoP	1.51	24@20	[31]
CoFe-LDH@NiSe	1.51	120@10	[32]
Fe-Ni_2P/CeO_2	1.52	120@1000	[33]
MXene@RuCo NPs	1.52		[27]
Fe_2P-CoP/CeO_2-20	1.52	40@500	[34]
Mo-Ni_3S_2/NF	1.52	100@100	[15]
$FeCoCrCuO_x$@CF	1.528	100@500	[12]
Co_2P-Ni_3S_2/NF	1.54	24@100	[29]
Mo-NiS_x@NiFe-LDH/NF	1.54	72@200	[22]
MoP-Mo_2C/NPC	1.55	168@100	[28]
$CoTe_2$/CoP	1.55	12@50	[7]
Ni_2P@C/NF	1.55	48@10	[16]
NiFeCd-LDH	1.57	25@10	[35]
Mn-W-CoP/NF	1.57	48@15	[11]
$Co_1Mo_1Ni_{0.5}P_i$	1.59	100@100	[36]
Fe-NiP	1.59	60@10	[19]
CoP/FeP/CP	1.62	60@10	[37]
B-CoO/Co@NC/NF(Ar)	1.62	100@10	[38]
N-$NiMoO_4$/Ni/CNTs	1.64	12@10	[39]
CoP/$Ti_3C_2T_x$	1.66	24@10	[40]
Mn-CP NTs	1.67	60@10	[41]

Table S4. ICP-OES analysis of element content before and after OER stability test reaction of FeP-Ni_2P-CoP/NF.

Sample	Fe(Wt%)	Co(Wt%)	Ni(Wt%)	Composition
Before	4.21	8.05	87.47	FeP-Ni_2P-CoP/NF
After	2.59	5.73	90.00	FeP-Ni_2P-CoP/NF

Table S5. The content of the metal ions in the electrolyte after OER determined by ICP-OES.

elements	**Fe**	**Co**	**Ni**
mg/L	0.065	0.024	0.009

Table S6. Atomic ratio of element in the FeP-Ni_2P-CoP/NF before and after HER determined by XPS.

Catalyst	Atomic ratio of element (%)					
	Co^{3+}	Co^{2+}	Fe^{3+}	Fe^{2+}	Ni^{3+}	Ni^{2+}
Initial	74.86	25.14	63.16	36.85	64.11	35.88
After HER	64.5	35.5	32.83	67.18	44.62	55.38

References

1. Y. Xu, J. Yang, T. Liao, R. Ge, Y. Liu, J. Zhang, Y. Li, M. Zhu, S. Li and W. Li, Bifunctional water splitting enhancement by manipulating Mo-H bonding energy of transition Metal-Mo_2C heterostructure catalysts, *Chem. Eng. J.,* 2022, **431**, 134126.
2. J. Qian, X. Wang, H. Jiang, S. Li, C. Li, S. Li, R. Ma and J. Wang, Surface Engineering of Cr-Doped Cobalt Molybdate toward High-Performance Hydrogen Evolution, *ACS Appl. Mater. Interfaces*, 2022, **14**, 18607–18615.
3. H. Xiong, C. Du, Z. Ma, R. Zhi, S. Hao, X. Zhao, Z. Liu, F. Xu and H. Wang, Rational Design of Multiple Heterostructures with Synergistic Effect for Efficient and Stable Hydrogen Evolution Toward Industrial Alkaline Water Splitting, *Adv. Funct. Mater.*, 2024, **34**, 2402298.
4. X. Luo, L. Wang, W. Sun, Z. Yang, P. Zhang, X. Chen and G. Liu, One-Step Electrodeposition of NiMoP/NF as an Efficient and Cost-Effective Cathodic Electrocatalyst for Alkaline Water Electrolysis, *Ind. Eng. Chem. Res.*, 2023, **62**, 10454–10466.
5. Y. Cao, X. Yin, Y. Gan, Y. Ye, R. Cai, B. Feng, Q. Wang, X. Dai and X. Zhang, Coupling effect and electronic modulation for synergistically enhanced overall alkaline water splitting on bifunctional Fe-doped CoB_i/CoP nanoneedle arrays, *J. Colloid Interface Sci.*, 2023, **652**, 1703-1711.
6. I. K. Mishra, H. Zhou, J. Sun, F. Qin, K. Dahal, J. Bao, S. Chen and Z. Ren, Hierarchical CoP/Ni_5P_4/CoP microsheet arrays as a robust pH-universal electrocatalyst for efficient hydrogen generation†, *Energy Environ. Sci.*, 2018, **11**, 2246-2252.
7. L. Yang, X. Cao, X. Wang, Q. Wang and L. Jiao, Regulative electronic redistribution of $CoTe_2$/CoP heterointerfaces for accelerating water splitting, *Appl. Catal. B Environ. Energy*, 2023, **329**, 122551.
8. X. Xia, G. Zhao, Q. Yan, B. Wang, Q. Wang and H. Xie, High-Density Defects Activating Fe-Doped Molybdenum Sulfide@N-Doped Carbon Heterostructures for Efficient Electrochemical Hydrogen Evolution, *ACS Sustain. Chem. Eng.,* 2022, **10**, 182–193.

9. C.-C. Cheng, T.-Y. Lin, Y.-C. Ting, S.-H. Lin, Y. Choi and S.-Y. Lu, Metal-organic frameworks stabilized Mo and W binary single-atom catalysts as high performance bifunctional electrocatalysts for water electrolysis, *Nano Energy*, 2023, **112**, 108450.

10. T. Li, H. Chen, Z. Chen, Z. Xue, X. Zhang and B. Hui, Scale-Up Preparation of Flexible Ni–W–P@Fiber Cloth Electrode for Boosting Overall Water Electrosplitting, *ACS Sustain. Chem. Eng.*, 2023, **11**, 14549–14558

11. Y. Zhao, X. Zhao, Y. Zhou, S. Zhao, J. Chen, R. Dai, W. Zhou, P. Yang, H. Zhang and A. Chen, Bimetallic co-doped CoP nanoflower arrays for efficient and stable overall water splitting, *Int. J. Hydrogen Energy*, 2024, **51**, 276-284.

12. C. Liu, J. Feng, P. Zhou, D. Liu, L. Qiao, D. Liu, Y. Cao, S.-C. Su, H. Liu and H. Pan, Multi-metal interaction boosts reconstructed $FeCoCrCuO_x$@CF toward efficient alkaline water electrolysis under large current density, *Chem. Eng. J.*, 2023, **476**, 146710.

13. D. Kong, Q. Xu, N. Chu, H. Wang, Y. V. Lim, J. Cheng, S. Huang, T. Xu, X. Li, Y. Wang, Y. Luo and H. Y. Yang, Rational Construction of 3D Self-Supported MOF-Derived Cobalt Phosphide-Based Hollow Nanowall Arrays for Efficient Overall Water Splitting At large Current Density, *Small*, 2024, **20**, 2310012.

14. M. Qin, G. Ma, W. Tan, Z. Fan and X. Xin, Constructing an n-n junction between CoFe-LDH and NiCoP as bifunctional electrocatalysts for efficient overall water splitting, *Inorg. Chem. Front.*, 2023, **10**, 4819-4828.

15. Y. Gao, W. He, D. Cao, F. Wang, Y. Li, Q. Hao, C. Liu and H. Liu, Mo-Doped Ni_3S_2 Nanosheet Arrays for Overall Water Splitting, *ACS Appl. Nano Mater.*, 2023, **6**, 6066-6075.

16. N. Chen, S. Che, H. Liu, G. Li, N. Ta, F. J. Chen, B. Jiang, N. Wu, Z. Li, W. Yu, F. Yang and Y. Li, Multistage interfacial engineering of 3D carbonaceous Ni_2P nanospheres/nanoflowers derived from Ni-BTC metal-organic frameworks for overall water splitting, *J. Colloid Interface Sci.*, 2023, **638**, 582-594.

17. K. Zhang, Y. Duan, N. Graham and W. Yu, Unveiling the synergy of polymorph heterointerface and sulfur vacancy in NiS/Ni_3S_2 electrocatalyst to promote alkaline hydrogen evolution reaction, *Appl. Catal. B Environ. Energy*, 2023, **323**, 122144.

18. N. Yang, W. Yang, X. Yang, X. Xiao, L. Zhang and L. Zhang, 2D/3D hierarchical and

multi-heterostructured Co/Ni/Fe phosphosulfide as a highly efficient bifunctional electrocatalyst for overall water splitting, *Int. J. Hydrogen Energy*, 2024, **56**, 396-405.

19. J. Zhou, C. Huang, Q. Zhou, Y. Xie, L. Yang, L. Yu and Y. Yu, Electronic Structure Regulation of Nickel Phosphide for Efficient Overall Water Splitting, *Inorg. Chem.*, 2022, **61**, 9318–9327

20. Q. Li, J. Bi, Y. Yao, X. Li and D. Xu, A novel 3D CoNiCu-LDH@CuO micro-flowers on copper foam as efficient electrocatalyst for overall water splitting, *Appl. Surf. Sci.*, 2023, **622**, 156874.

21. Y. Li, X. Yu, J. Gao and Y. Ma, Structural and electronic modulation of $(Fe,Ni)_2P@Ni_2P$ heterostructure for efficient overall water splitting at high current density, *Chem. Eng. J.*, 2023, **470**, 144373.

22. Y. Li, H. Guo, Y. Zhang, H. Zhang, J. Zhao and R. Song, Hollow Mo-doped NiS_x nanoarrays decorated with NiFe layered double-hydroxides for efficient and stable overall water splitting, *J. Mater. Chem. A*, 2022, **10**, 18989-18999.

23. Y. Wei, L. Yi, R. Wang, J. Li, D. Li, T. Li, W. Sun and W. Hu, A Unique Etching-Doping Route to Fe/Mo Co-Doped Ni Oxyhydroxide Catalyst for Enhanced Oxygen Evolution Reaction, *Small*, 2023, **19**, 2301267.

24. Y. Gao, H. Ding, X. Fan, J. Xiao, L. Zhang and G. Xu, Anchoring cobalt molybdenum nickel alloy nanoparticles on molybdenum dioxide nanosheets as efficient and stable self-supported catalyst for overall water splitting at high current density, *J. Colloid Interface Sci.*, 2023, **648**, 745-754.

25. K. Chang, D. T. Tran, J. Wang, K. Dong, S. Prabhakaran, D. H. Kim, N. H. Kim and J. H. Lee, Triphasic Ni_2P-Fe_2P-CoP heterostructure interfaces for efficient overall water splitting powered by solar energy, *Appl. Catal. B Environ. Energy*, 2023, **338**, 123016.

26. T. Niyitanga, J. W. Choi and H. Kim, Hierarchical 3D porous trimetallic palladium-iron and cobalt on nickel foam as electrocatalyst for large current density oxygen evolution reaction in alkaline seawater, *J. Colloid Interface Sci.*, 2024, **657**, 229-239.

27. J. Li, C. Hou, C. Chen, W. Ma, Q. Li, L. Hu, X. Lv and J. Dang, Collaborative Interface Optimization Strategy Guided Ultrafine RuCo and MXene Heterostructure Electrocatalysts for Efficient Overall Water Splitting, *ACS Nano*, 2023, **17**, 10947-10957.

28. E. Jiang, J. Li, X. Li, A. Ali, G. Wang, S. Ma, J. Zhu and P. K. Shen, MoP-Mo_2C quantum dot heterostructures uniformly hosted on a heteroatom-doped 3D porous carbon sheet network as an efficient bifunctional electrocatalyst for overall water splitting, *Chem. Eng. J.*, 2022, **431**, 133719.

29. H. Li, X. Gao and G. Li, Construction of Co_2P-Ni_3S_2/NF Heterogeneous Structural Hollow Nanowires as Bifunctional Electrocatalysts for Efficient Overall Water Splitting, *Small*, 2023, **19**, 2304081.

30. C. Zhang, Y. Han, W. Wang, R. Huang, R. Ma and J. Yan, Engineering MIL-88A-Derived Self-Supported Moss-like Iron Phosphide Particles on Nickel Foam as Robust Bifunctional Electrocatalysts for Overall Water Splitting, *ACS Appl. Energy Mater.*, 2022, **5**, 9392-9401.

31. Y. Dong, Z. Deng, Z. Xu, G. Liu and X. Wang, Synergistic Tuning of CoO/CoP Heterojunction Nanowire Arrays as Efficient Bifunctional Catalysts for Alkaline Overall Water Splitting, *Small Methods*, 2023, **7**, 2300071.

32. D. Kim, Y. Lee, M. Kim, G. Lee and S. M. N. Jeghan, Designing a smart heterojunction coupling of cobalt-iron layered double hydroxide on nickel selenide nanosheets for highly efficient overall water splitting kinetics, *Appl. Catal. B Environ. Energy*, 2022, **308**, 121221.

33. Y. Huang, X. Ding, B. Huang and Z. Xie, CeO_2-decorated Fe-doped Ni_2P nanosheets for efficient electrocatalytic overall water splitting at high current densities, *J. Alloys Compd.*, 2024, **981**, 173672.

34. X. Ding, J. Yu, W. Huang, D. Chen, W. Lin and Z. Xie, Modulation of the interfacial charge density on Fe_2P-CoP by coupling CeO_2 for accelerating alkaline electrocatalytic hydrogen evolution reaction and overall water splitting, *Chem. Eng. J.*, 2023, **451**, 138550.

35. Q. Liu, K. Chen, M. Wang, H. Fan, Z. Yan, X. Du and Y. Chen, In-situ construction of cation vacancies in amphoteric-metallic element-doped NiFe-LDH as ultrastable and efficient alkaline hydrogen evolution electrocatalysts at 1000 mA cm^{-2}, *J. Colloid Interface Sci.*, 2024, **663**, 624-631.

36. P. Viswanathan and K. Kim, In Situ Surface Restructuring of Amorphous Ni-Doped

CoMo Phosphate-Based Three-Dimensional Networked Nanosheets: Highly Efficient and Durable Electrocatalyst for Overall Alkaline Water Splitting, *ACS Appl. Mater. Interfaces*, 2023, **15**, 16571-16583.

37. L. Zeng, L. An, Z. Zhang, J. Zheng, W. Chen, C. Liu, Y. Zheng, D. Dang and Z.-Q. Liu, Heterogeneous strategy constructing a built-in electric field: CoP/FeP bifunctional electrode for overall water splitting, *Chem. Eng. J.*, 2024, **491**, 152084.

38. D. C. Cha, T. I. Singh, A. Maibam, T. H. Kim, D. H. Nam, R. Babarao and S. Lee, Metal-Organic Framework-Derived Mesoporous B-Doped CoO/Co@N-Doped Carbon Hybrid 3D Heterostructured Interfaces with Modulated Cobalt Oxidation States for Alkaline Water Splitting, *Small*, 2023, **19**, 2301405.

39. G.-L. Li, X.-Y. Qiao, Y.-Y. Miao, T.-Y. Wang and F. Deng, Synergistic Effect of N-$NiMoO_4$/Ni Heterogeneous Interface with Oxygen Vacancies in N-$NiMoO_4$/Ni/CNTs for Superior Overall Water Splitting, *Small*, 2023, **19**, 2207196.

40. B. Liu, P. Zhao, Z. Wu, C. Liu, H. Jing, J. Song, K. Lu, W. Lei and Q. Hao, Prussian blue analogue-derived CoP nanocubes supported on MXene toward an efficient bifunctional electrode with enhanced overall water splitting, *J. Colloid Interface Sci.*, 2024, **661**, 709-719.

41. F. Tang, Y. W. Zhao, Y. Ge, Y.-G. Sun, Y. Zhang, X.-L. Yang, A.-M. Cao, J.-H. Qiu and X.-J. Lin, Synergistic effect of Mn doping and hollow structure boosting Mn-CoP/Co_2P nanotubes as efficient bifunctional electrocatalyst for overall water splitting, *J. Colloid Interface Sci.*, 2022, **628**, 524-533.